

On the aberration–retardation effects in pulsars

K. Krzeszowski,^{1*} D. Mitra,² Y. Gupta,² J. Kijak,¹ J. Gil¹ and A. Acharyya³

¹*J. Kepler Institute of Astronomy, University of Zielona Góra, Lubuska 2, 65–265, Zielona Góra, Poland*

²*National Centre for Radio Astrophysics, TIFR, Pune University Campus, Post Bag 3, Ganeshkind PO, Pune, Maharashtra 411007, India*

³*School of Electronics and Computer Science, University of Southampton, Southampton SO17 1BJ*

Accepted 2008 November 24. Received 2008 November 17; in original form 2008 October 4

ABSTRACT

The magnetospheric locations of pulsar radio emission region are not well known. The actual form of the so-called radius-to-frequency mapping should be reflected in the aberration–retardation (A/R) effects that shift and/or delay the photons depending on the emission height in the magnetosphere. Recent studies suggest that in a handful of pulsars the A/R effect can be discerned with respect to the peak of the central core emission region. To verify these effects in an ensemble of pulsars, we launched a project analysing multifrequency total intensity pulsar profiles obtained from the new observations from the Giant Meterwave Radio Telescope (GMRT), Arecibo Observatory (AO) and archival European Pulsar Network (EPN) data. For all these profiles, we measure the shift of the outer cone components with respect to the core component, which is necessary for establishing the A/R effect. Within our sample of 23 pulsars, seven show the A/R effects, 12 of them (doubtful cases) show a tendency towards this effect, while the remaining four are obvious counterexamples. The counterexamples and doubtful cases may arise from uncertainties in the determination of the location of the meridional plane and/or the core emission component. Hence, it appears that the A/R effects are likely to operate in most pulsars from our sample. We conclude that in cases where those effects are present the core emission has to originate below the conal emission region.

Key words: radiation mechanism: non-thermal-methods: data analysis – stars: neutron – pulsars: general.

1 INTRODUCTION

Aberration and retardation effects (A/R) can be observed in a pulsar profile as a shift of the position of conal components with respect to the core component towards earlier longitudinal phases (see e.g. Malov & Suleimanova 1998; Gangadhara & Gupta 2001, hereafter G&Ga). Such effects should occur if different components are emitted at different distances from the pulsar surface (emission radii), as well as from the pulsar spin axis. Aberration is caused by bending of radiation beam due to the polar cap rotation, while retardation is based on a path difference for radiation from different conal emission regions to reach an observer. If we assume that the emission from the core component arises relatively close to the star surface, then it should not be strongly affected by either of the two above-mentioned effects. This will be our initial assumption.

To determine A/R shifts, the pulsar profile has to meet certain requirements. It has to be a high-resolution profile with high signal-to-noise ratio (S/N). The core and the conal components have to be clearly identified within the profile. Multifrequency data are recommended, so one can follow the profile evolution throughout all

frequencies, which can help to identify different emission components.

When values of A/R shifts are determined, then the heights of the radiation emission region (emission altitudes hereafter) can be calculated (see G&Ga and Dyks, Rudak & Harding 2004). It is believed that at different frequencies the emission arises at different heights above the pulsar surface (Kijak & Gil 1998, 2003; Mitra & Rankin 2002). The results of this analysis can be used to verify the existence of a radius-to-frequency mapping. Hence, all observational limits for emission altitude can be crucial for understanding the physical mechanism of generation of pulsar coherent radio emission.

The relativistic beaming model initially proposed by Blaskiewicz, Cordes & Wasserman (1991, hereafter BCW) clearly demonstrated that A/R effects play an important role in pulsars. This study was primarily based on the evidence that followed from the effects of A/R as seen in the inflexion point of the pulsar’s polarization position angle (PA) traverse, which lags the mid-point of the total intensity profile centre. A similar effect of A/R was reported by G&Ga and Gupta & Gangadhara (2003, hereafter G&Gb) in a handful of pulsars where the core emission was seen to lag behind the profile centre.

In this paper, we have undertaken a careful study to establish the A/R effect observed by G&Ga and G&Gb for a large sample of

*E-mail: chriss@astro.ia.uz.zgora.pl

pulsars observed at multiple frequencies. Most of the data are new observations from the Giant Meterwave Radio Telescope (GMRT) and the Arecibo Observatory (AO). We have also used some archival data from the European Pulsar Network (EPN) archive.¹ In Section 2 we discuss various methods used to find emission heights in pulsars, in Section 3 we discuss various factors affecting A/R measurements in pulsars and Section 4 deals with the observation and data analysis methods used in this paper.

As a result of our analysis presented in Section 5, we found that out of 23 pulsars in our sample seven clearly show the A/R effect, 12 show a clear tendency towards this effect, while the remaining four are counterexamples. However, as argued in Section 3, all problematic cases (pulsar profiles at all or some frequencies not showing the A/R effect) can be attributed to a number of effects like incorrect identification of the core component or missing conal emission. We can conclude that A/R effects are seen to operate in pulsars, which we discuss in Section 6.

2 GEOMETRY AND EMISSION ALTITUDES

Radio emission heights in pulsars are primarily obtained by two methods: the geometrical method and heights estimation based on A/R effects. Here, we briefly mention the essential ingredients of the methods used, and a detailed discussion of the various methods used can be found in Mitra & Li (2004).

Radio emission geometry is determined by several parameters: α – an inclination angle of the magnetic dipole with respect to the rotation axis, β – the minimum angle between an observer’s line of sight and magnetic axis (impact angle), ρ – an opening angle of the radio emission beam, r – a radial distance of the radio emission region measured from the centre of the neutron star (emission altitude). The opening angle ρ of the pulsar beam corresponding to the pulse width W is given by

$$\rho = 2 \arcsin \left(\sqrt{\sin(\alpha + \beta) \sin \alpha \sin^2 \frac{W}{4} + \sin^2 \frac{\beta}{2}} \right), \quad (1)$$

where α , β , W and ρ are measured in degrees (Gil, Gronkowski & Rudnicki 1984). The opening angle ρ is the angle between the pulsar magnetic axis and the tangent to magnetic field lines at points where the emission corresponding to the apparent pulse width W originates. For dipolar field lines,

$$\rho = 1.24 s (r/10^6 \text{ cm})^{1/2} P^{-1/2} \quad (2)$$

(Gil & Kijak 1993), where $s = d/r_p$ is a mapping parameter which describes the locus of corresponding field lines on the polar cap ($s = 0$ at the pole and $s = 1$ at the edge of the polar cap), d is the distance of the given magnetic open field line from the dipolar magnetic axis (in cm), r_p is the polar cap radius (in cm) and P is the pulsar period in seconds. The radio emission altitude can be obtained using equation (2):

$$r_{\text{geo}} \simeq 10P \left(\frac{\rho}{1.24} \right)^2 \text{ km}. \quad (3)$$

In this equation, parameter $s = 1$ is used which corresponds to the bundle of last open magnetic field lines. Kijak & Gil (1997) also derived a semi-empirical formula for emission height which was slightly modified by Kijak & Gil (2003) by using larger number of pulsars and broadening the frequency coverage in their analysis. They estimated the emission heights for a number of pulsars at

several frequencies using the geometrical method (equations 1 and 3) based on the above assumption that the low-intensity pulsar radiation (corresponding to the profile wings) is emitted tangentially to the bundle of the last open dipolar field lines. In the method, they used low-intensity pulse width data at about 0.01 per cent of the maximum intensity (Kijak & Gil 1997, 2003). The most recent formula has a form

$$r_{\text{KG}} = (400 \pm 80) \nu_{\text{GHz}}^{-0.26 \pm 0.09} \dot{P}_{-15}^{0.07 \pm 0.03} P^{0.30 \pm 0.05} \text{ km}, \quad (4)$$

where ν_{GHz} is observing frequency in GHz and $\dot{P}_{-15} = \dot{P}/10^{-15}$ is the period derivative. The formula r_{KG} sets lower and upper boundaries for emission height values in the statistical sense.

For calculating the emission heights, one can take a different approach. The A/R effects have been observed in the total intensity profiles as discussed by Malov & Suleimanova (1998), G&Ga, G&Gb and Dyks et al. (2004). In turn, they have been used to calculate radio emission heights. Observationally, the A/R effects are obtained by measuring the positions of the conal emission components and identifying the central core emission component. The shape of the observed profile depends on the structure of radio beam, which is thought to be composed of a central core emission surrounded by nested cones (Rankin 1983; Mitra & Deshpande 1999). The line of sight passing through the central region of this beam will hence cut the cone emission at the edges including the central core region. Following this, pulsar profiles can be classified due to the number and type of visible components (Rankin 1983). If we assume that in a certain profile the core component and both the conal components are present, we can define the phase difference:

$$\Delta\phi = \frac{\phi_t - |\phi_l|}{2}, \quad (5)$$

where ϕ_l and ϕ_t are phase positions (in degrees) of the peaks of the leading and trailing components with respect to the core phase ($\phi_c = 0^\circ$). Following the refinement of G&Ga by Dyks et al. (2004), one can estimate the radio emission altitude,²

$$r_{\text{AR}} \simeq -\frac{\Delta\phi}{2} \frac{2\pi}{360^\circ} R_{\text{LC}}, \quad (6)$$

where $R_{\text{LC}} = cP/2\pi$ (where c is speed of light) is the light cylinder radius. The A/R method has an edge over the geometrical method since it only depends weakly on the geometrical angles of the star that are difficult to find. Generally, the emission altitudes found using both these methods are of the order of a few hundred kilometres above the surface of the neutron star. In this paper, we use equation (6) for estimating emission altitudes following the method outlined by G&Ga. The various factors affecting the usage of this method are discussed in Section 3.

3 FACTORS AFFECTING A/R MEASUREMENTS IN PULSARS

3.1 Location of the meridional point

The crucial aspect for estimating radio emission heights using the A/R technique is to identify the location of the meridional plane,

² Recently in a detailed study, Gangadhara (2005) has obtained a revised expression (their equation 34) for the relativistic phase shift, which depends on the angles α and β , and the corrections in obtaining emission heights turn out to be of the order of 2–10 per cent for normal pulsars. We have, however, not used this formula since all the pulsars in our sample are normal pulsars and, further, the errors in estimating emission heights are often more than 10 per cent.

¹ <http://www.mpifr-bonn.mpg.de/div/pulsar/data/>

i.e. the plane containing the magnetic axis and the pulsar rotation axis.

Generally, polarization observations have been used to identify the meridional plane as per the rotating vector model (RVM) proposed by Radhakrishnan & Cooke (1969). According to the RVM, the variation of the PA of the linear polarization across the pulse reflects the underlying structure of the dipolar magnetic field if one is located on the pulsar frame. In this case, the steepest gradient or the inflexion point of the PA traverse is the point contained in the meridional plane, and should be coincident with the mid-point of the pulse profile. However in the observer's frame, as was pointed out by BCW and Dyks et al. (2004), the A/R effects cause the PA inflexion point to appear delayed with respect to the mid-point of the pulse profile. The magnitude of the delay is proportional to the height of emission from the neutron star surface and inversely proportional to the pulsar period. Hence, in the observer's plane the inflexion point of the PA traverse is no longer the point containing the meridional plane, rather the meridional plane lies somewhere in between the profile mid-point and the inflexion point of the PA traverse.

We use the method employed by G&Ga and G&Gb to find emission heights due to A/R effects using equation (6). If the mid-point of the outer conal peaks leads the core peak, it would imply that the conal emission is higher than the core emission and the shift can be used to find emission heights with respect to the core. This argument, however, assumes that the meridional plane passes through the peak of the core emission. While this assumption is not rigorously verified, there are few pulsars that have been used to justify this argument. One such pulsar is PSR B1857–26 (see Fig. 1), where the peak of the core, the inflexion point and the sign-changing circular are all close to each other (see Mitra & Rankin 2008 for a detailed discussion). If one assumes that the core emission is curvature radiation that fills the full polar cap as was suggested by Rankin (1990), then the meridional plane would lie in the plane containing the inflexion point, peak of the core and sign-changing circular. Although a critical look at PSR B1857–26 reveals that the peak of the core is delayed by a degree or so with respect to the inflexion point (see Mitra & Rankin 2008). Mitra & Li (2004) have shown that for a few other pulsars the peak of the core lags the inflexion point by about a degree. The shifts expected due to A/R effects for slow pulsars are also often small (e.g. for emission altitude of 300 km and a 0.7 s pulsar, the expected shift is of the order of a degree) and is comparable to core shifts seen with respect to the inflexion point.

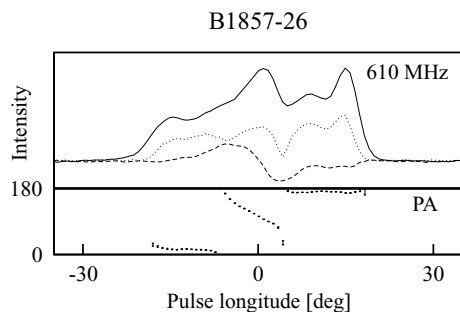


Figure 1. B1857–26 polarization profile. The upper panel of the plot shows the intensity (solid line), linear polarization (dotted line) and the circular polarization (dashed line). The bottom panel shows the PA with error bars. This profile is an example where the core component, the inflexion point and the sign-changing circular are close to each other (see Section 3 for details).

Hence, it is important to note that to demonstrate the A/R effects as suggested by G&Ga and G&Gb, the meridional plane should pass through the peak of the core emission (which is currently not verified) and the conal emission should be rising higher than the core emission.

3.2 Identifying the core emission

Identification of the core emission is not trivial in pulsars. Under the core-cone model of pulsar beaming, the core is centrally located and surrounded by nested cones. This implies that the core is located in the centre of a pulse profile, which is very close to the inflexion point of the PA. Since the impact parameter needs to be small to cut through the core emission region in a pulsar, the corresponding PA traverse as per the RVM should show a significant rotation across the pulse. Core emission is often associated with a sign-changing circular polarization and has a steeper spectral index than the conal emission.

There are situations where several core-like emission characteristics are seen in a pulse component. For example, in Fig. 2 PSR B1831–04 has a bright central component, which is identified as core emission by Rankin (1993a,b). This component has a steep spectral index and a sign-changing circular as seen in Gould & Lyne's (1998, hereafter GL98) multifrequency polarization profiles. On the other hand, the PA traverse is flat, showing no significant rotation (except 90° jumps) and the profile is extremely wide ($\sim 150^\circ$). Such emission properties are consistent with the observer crossing the pulsar emission beam along the conal emission zone and the observer is likely to miss the core emission. Hence, for PSR B1831–04, the bright centrally located component can be interpreted as conal emission rather than core emission. Further, there are situations where the PA below the core emission can deviate from the RVM model (see Mitra, Rankin & Gupta 2007), and hence the location of the inflexion point is difficult to determine. A careful examination using multifrequency single pulse polarization data is hence essential to find the location of the core emission. For our data set, we have used the GL98 polarization data sets wherever possible to find the location of the core emission, which we discuss in the Appendix. However, incorrect identification of the core would clearly affect the demonstration of the A/R effect.

In several cases, the central emission close to the core is weaker compared to the outer cones. Methods employed to find the peak of the core (like the Gaussian-fitting scheme discussed in Section 4) have problems in establishing the location of the core component

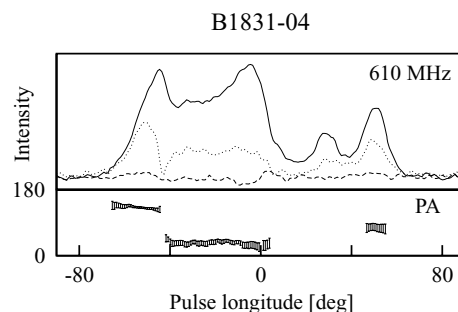


Figure 2. B1831–04 polarization profile (same as in Fig. 1). Although this pulsar shows the sign change in circular, it has a flat PA and a wide profile. Hence, it is likely that the central bright emission component is not a core (see Section 3 for details).

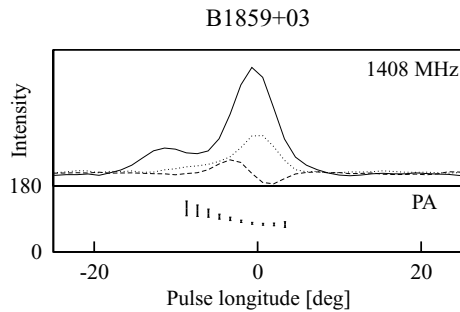


Figure 3. B1859+03 polarization profile (same as in Fig. 1). This pulsar has a clear sign-changing circular indicating the location of the core emission. However, the emission towards the trailing parts of the profile seems to be missing (see Section 3 for details).

(like PSR B1738–08), and hence cause complication in discerning the A/R effect.

Subpulse modulation (or drifting) provides another means to identify core and conal components in pulsars. The conal components tend to show subpulse drifting seen as a spectral feature in phase-resolved fluctuation spectra, while in the core emission this phenomenon is generally absent (Rankin 1986). It is sometimes possible that the central component of the pulsar shows drifting properties, in which case the central component cannot be core emission. We have verified our sample pulsars for such drifting of the central component based on the data set of pulsar subpulse modulation published by Weltevrede, Stappers & Edwards (2006) and Weltevrede, Edwards & Stappers (2007). Three pulsars from our sample show central component modulation feature out of which two pulsars PSR B1508+55 and B1917+00 have a broad modulation feature, which is consistent with core emission, while PSR B1944+17 shows clear drifting properties making this pulsar unsuitable for the A/R analysis.

3.3 Partial cone emission

In several pulsars, only a part of the emission cone is visible and these pulsars were identified as partial cones by Lyne & Manchester (1988). The PA inflexion point in these pulsars lies towards one edge of the profile. This kind of pulsar, however, poses a problem for finding the A/R effect, since estimation of the mid-point of the total intensity profile is incorrect due to missing emission. One such example in our sample is perhaps PSR B1859+03 as shown in Fig. 3. The PA inflexion point coincides with the peak of the trailing component and has a sign-changing circular, which is suggestive of core emission; however, there is no emission component seen in the trailing part of the profile. A single-pulse study by Mitra, Rankin & Sarala (2008) recently has shown that the missing partial cone regions occasionally flare up, and these flared profiles can be used to demonstrate the A/R effect.

4 OBSERVATIONS AND DATA ANALYSIS

For our analysis, we selected profiles of 28 pulsars from three sources (see Table 1): GMRT, AO and EPN. The GMRT (Swarup et al. 1991) operating at metre wavelengths is an array of 30 antennas with alt-az mounts, each of 45-m diameter, spread out over a 25-km region located 80 km north of Pune, India. It is designed to operate at multiple frequencies (150, 235, 325, 610 and 1000–1450 MHz, respectively), having a maximum bandwidth of 32 MHz

split into upper and lower sidebands of 16 MHz each. It is primarily an aperture synthesis interferometer as well as a phased array instrument. The GMRT observations reported in this paper are done in the phased array mode of operation at RF 225 and 325 MHz, respectively, using the upper sideband and a bandwidth of 16 MHz. In the phased array mode of the GMRT (Gupta et al. 2000; Sirothia 2000), signals from any selected set of the antennas are added together after an appropriate delay and phase compensation to synthesize a single, larger antenna with a narrower beam. Signals of 16 MHz from each sideband of each antenna are available across 256 channels, which can be summed in the GMRT array combiner. The summed voltage signal output from the phased array is then processed like any other single dish telescope signal, by the pulsar back end. At the frequencies of interest here, GMRT has two linearly polarized outputs for each antenna, which are further mixed in a quadrature hybrid to produce two circular polarized signals which go further into the front-end electronics and rest of the signal chain. The raw signals are finally post-integrated by the pulsar back end and the data were recorded with the final sampling time of 0.512 ms. The time resolution for all the analysis done in this paper is the pulsar period divided by the sampling time. All the pulsars were observed for about 2000 pulse periods to obtain stable pulse profiles. The off-line analysis involved interference rejection, dedispersion and folding to obtain the average pulse profiles.

The AO data set is from observations at the Arecibo Observatory, carried out between 2001 December and 2002 June. The pulsars were observed at different frequencies using the following receivers: 430 MHz, *L* band (1175 MHz), *S* low (2250 MHz), *S* high (3500 MHz), *C* band (4850–5000 MHz). The pulsar back end used most frequently was the Wideband Arecibo Pulsar Processor (WAPP), though the Penn State Pulsar Machine (PSPM) was also used for some of the observations. The bandwidths of the observations were typically 25/50 MHz at 430 MHz and 100 MHz for all the higher frequency observations. The time resolution of the WAPP raw data was typically 128, 256 or 512 μ s. The data were analysed using the SIGPROC analysis package to get the average folded profiles.

The data from the EPN archive were mostly obtained by GL98 using 76-m Lovell telescope at Jodrell Bank Observatory, except B1039–19 at 4850 MHz, which was obtained by Kijak et al. (1997) using Effelsberg Observatory. Generally, resolution of EPN data is around 1° , which is much lower than that of GMRT or AO data.

Our analysis followed these steps: (1) identification of core components in profiles. We have used several established methods for discriminating the core components: (i) quasi-centrality of the component flanked by one or two pairs of conal components, (ii) associating the core component with the inflexion point of the PA traverse and sense-reversing signature of circular polarization under the core component (although the polarimetry was not always available in our data); (2) identification of conal pairs as leading and trailing components, primarily based on symmetric location of components on either side of the core one; (3) estimation of phase shifts according to equation (5) and (4) estimation of the emission heights according to equation (6). This simple procedure is not always straightforward in practice. There are cases when components merge (especially as a function of the observing frequency) and their positions are not clearly determined. In these cases, we decided to use a Gaussian-fitting method introduced by Kramer et al. (1994). For consistency, we applied this method to all our profiles, even those in which all components were clearly distinguishable. The Gaussian-fitting procedure was as follows: fix Gaussian parameters of identifiable components (position, amplitude, width),

Table 1. List of pulsars chosen for analysis. The AO and GMRT observations are new, whereas the EPN profiles have been taken from the data archive <http://www.mpifr-bonn.mpg.de/div/pulsar/data/>.

Pulsar	ν (MHz)	Data source	Pulsar	ν (MHz)	Data source	Pulsar	ν (MHz)	Data source	
B0402+61	225	GMRT	B1541+09	225	GMRT	B1911+13	325	GMRT	
	408	EPN		325	GMRT		445	AO	
B0410+69	225	GMRT	B1737+13	457	AO	B1916+14	1225	AO	
	408	EPN		1225	AO		445	AO	
B0621−04	325	GMRT	B1821+05	2300	AO	B2020+28	1225	AO	
	410	EPN		4900	AO		B1917+00	225	GMRT
	610	EPN		225	GMRT			325	GMRT
	1408	EPN		445	AO		B1944+17	225	GMRT
B0656+14	445	AO	457	AO	325	GMRT			
B0950+08	455	AO	B1738−08	1225	AO	B1946+35	2300	AO	
B1039−19	225	GMRT		225	GMRT		B2002+31	1225	AO
	325	GMRT	325	GMRT	2300	AO			
	1408	EPN	B1821+05	225	GMRT	B2020+28	445	AO	
4850	EPN	445		AO	B2053+21	445	AO		
B1237+25	157	GMRT	B1831−04	1225	AO	B2053+36	1225	AO	
	455	AO		1460	AO	B2315+21	225	GMRT	
	1225	AO		2200	AO		1225	AO	
	2300	AO		B1839+09	225	GMRT	B2319+60	225	GMRT
	3550	AO			325	GMRT		610	EPN
	4900	AO		606	EPN	925	EPN		
	5050	AO		B1839+09	2200	AO	1408	EPN	
B1508+55	225	GMRT	B1848+08	445	AO	1642	EPN		
	408	EPN	B1857−26	225	GMRT				
	610	EPN	B1859+03	1225	AO				
	925	EPN		2250	AO				
	1408	EPN							
	1642	EPN							

put additional Gaussian with some initial parameters and allow the fitting method to find the best position, amplitudes and widths. For detailed information about Gaussian-fitting method, see Kramer et al. (1994). After applying this method to unresolved components, we obtained a full and consistent set of component positions to be used in further analysis.

5 RESULTS

Our preliminary data set was reduced to 23 pulsars, because it was hard to perform a reasonable fitting on five pulsars (B0950+08, B1859+03, B1946+35, B2020+28, B2315+21) due to either low S/N or problems with determining positions of core and/or conal components, even using a Gaussian-fitting method. The determined positions of all components in a pulse profile, using the already mentioned Gaussian-fitting procedure, were used for a further analysis.

First, we estimate the phase shifts due to the A/R effect, and find the emission height r_{AR} using equation (6). For calculating the phase shifts using equation (5), we first identify the leading and trailing component of a cone of emission using the location of the peak of the Gaussian-fitted component as ϕ_l and ϕ_t [this profile measure is often called as peak-to-peak component separation (PPCS); see e.g. G&Ga and G&Gb, Dyks et al. 2004; Mitra & Li 2004]. Correspondingly, we denote the phase shift as $\Delta\phi_{PPCS}$. Wherever possible, $\Delta\phi_{PPCS}$ was estimated for the inner and outer cones separately.

To estimate errors of single-phase position measurements, we used the formula introduced by Kijak & Gil (1997):

$$\sigma = \tau \times \sqrt{1 + \left(\frac{\sigma_1}{I}\right)^2}, \quad (7)$$

where τ is the observing resolution, σ_1 is the root mean square of total intensity and I is the measured signal level. Since W estimations need two measurements (left- and right-hand side of profile at particular intensity level) and $\Delta\phi$ estimations need three measurements (ϕ_0 , ϕ_1 and ϕ_t), we took

$$\sigma_W = \sqrt{\sigma_l^2 + \sigma_r^2} \quad (8)$$

$$\sigma_{\Delta\phi} = \sqrt{\sigma_{\phi_0}^2 + \sigma_{\phi_1}^2 + \sigma_{\phi_t}^2} \quad (9)$$

as an error for W and $\Delta\phi$, respectively.

The best example of a pulsar whose apparent components are very well reproduced by the Gaussian-fitting method is PSR B1237+25 presented in Fig. 4 at a number of frequencies. All B1237+25 profiles are fitted perfectly with five Gaussian components, being an ideal example of applicability of the Gaussian-fitting technique used in this pulsar. This pulsar clearly shows the A/R effects at all frequencies consistently over the spectrum from about 5 to 0.16 GHz (see also Table A.5.2 in Section A.5 in the online Appendix). The profiles are arranged in panels with ascending frequency. The original profiles are plotted with solid lines, while the fitted Gaussian components are drawn with dashed lines. The profiles are aligned with respect to the peak of the central Gaussian component identified as the core component. All the profiles of pulsar B1237+25 show a clear A/R shift. Srostlik & Rankin (2005) have found that PA steepest gradient traverse lags the sign-changing circular polarization zero-point by about $0^\circ.4$. However, if one takes this value into account, B1237+25 still shows the A/R shift.

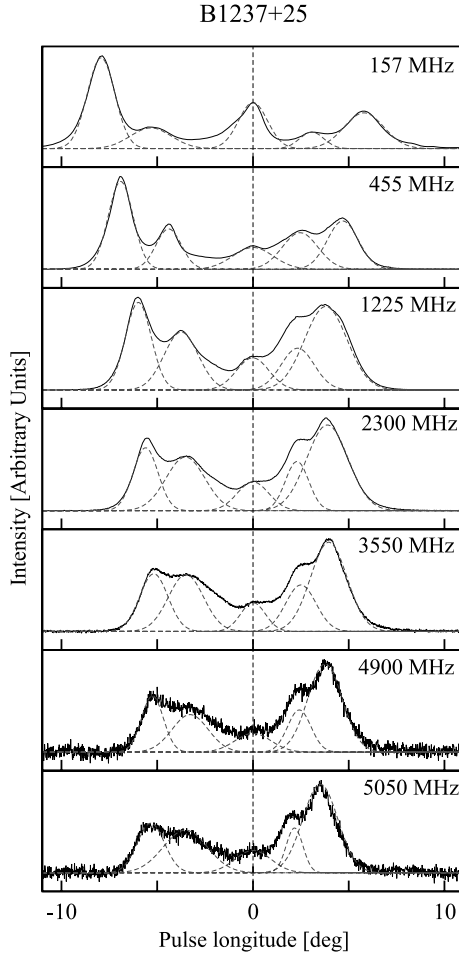


Figure 4. The profile evolution and fitted Gaussians of B1237+25 through a number of frequencies. This is a good example of showing clear A/R effects at all frequencies.

Our main results, which will be discussed later on, show the commonness of A/R effects in pulsar profiles. Within our sample of 23 pulsars, seven show clear A/R effects, 12 of them (doubtful cases) show a clear tendency towards this effect, while the remaining four are so-called counterexamples. When it comes to single $\Delta\phi$ measurements, we found that 45 measurements show negative shifts, which is expected for A/R effects, 23 measurements are doubtful within uncertainties, while remaining 19 show opposite shifts. However, taking into account only the outer cones (where more than one cone is seen) reveals that 30 shift measurements show A/R effects, 18 are doubtful cases, whereas 14 show no A/R effects at all. For the majority of non-A/R cases, the problem lies mostly in misidentifying core components. Some of the cases are partial cones, which also make it difficult to measure A/R shift properly. For a detailed discussion of various issues regarding A/R calculations, see Section 3. For a discussion of the results, see Section 6.

Note that all individual results are available in the form of figures and detailed tables in the electronic form as an appendix to this paper.

6 CONCLUSIONS AND DISCUSSION

Observationally, the peak of the core component lagging the centre of the outer conal component has always been considered as evidence for A/R effects operating in pulsars. Those effects have been demonstrated in a few pulsars so far: PSR B0329+54 by Malov & Suleimanova (1998) and G&Ga between 103 MHz to 10.5 GHz and PSRs B0450–18, B1237+25, B1821+05, B1857–26, B2045–16 and PSR B2111+46 at 325 MHz by G&Gb. In this work, our aim was to verify the A/R effects for a large sample of pulsars. While our sample consists of 23 pulsars, we note that our analysis is aided by using multifrequency measurements, where each frequency serves as an independent data set. Hence, although our sample consists of three pulsars common with G&Gb, the measurements are done at different frequencies and can be treated as independent check for their results. In our data set of 62 pulse profiles measured, the A/R effects are clearly seen in 30 profiles. Fig. 5 shows the distribution

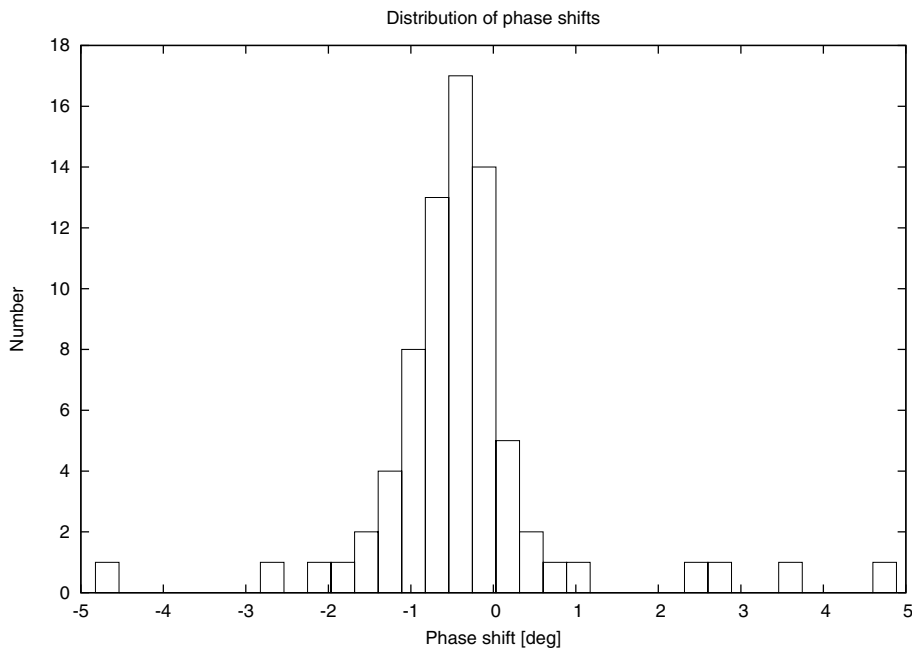


Figure 5. Distribution of measured phase shifts $\Delta\phi_{ppcs}$. Note that a clear tendency for negative shifts is seen in the sample.

of the measured phase shifts $\Delta\phi_{\text{PPCS}}$ for our sample of pulsars (for the data, see the Appendix). The tendency for the negative shift, which is the signature for A/R effect, is clearly visible.

Out of the four counterexamples noted in our sample, the most outstanding one is PSR B1831–04 (Fig. 2). We think that the central component in this pulsar might be incorrectly identified as the core emission (as discussed in Section 3). The flat PA traverse seems to suggest that the line of sight is not cutting the overall beam centrally (see another example of broad profile pulsar B0826–34 discussed by Gupta et al. 2004), so the core emission might be missing. If this is the case then the central component could arise from grazing the third innermost cone of emission, although its non-central location is a concern in this model. However, if our hypothetical third cone interpretation is incorrect, then B1831–04 remains the strongest counterexample of A/R effects.

The three other counterexamples, B1738–08, B1848+04 and B1859+03, show a marginal deviation from the A/R effects and are probably also related to our inability of identifying the location of the core component. In the first case (B1738–08), the core component is not apparent, although a blind Gaussian-fitting method indicates a central ‘core’ component (see Fig. A9 in the online Appendix). The second pulsar (B1848+04) is again a typical example of a broad profile pulsar (see Fig. A13 in the online Appendix), where the core component is likely to be missed. The third pulsar (B1859+03) (see Fig. A4 in the online Appendix) is a clear example of a pulsar with missing component (in this case, the trailing one). Therefore, we conclude that all the four cases

of strong counterexamples reported are the result of misidentification of the core component. Sometimes, weak conal emission or merged conal component leads to wrong identification of the emission components. For example, in PSR B1541+09 the leading conal component at 1225 and 2330 MHz is difficult to model. In cases like PSR B1944+17 and B1737+13, the weak conal emission poses difficulties in determining the location of the components. It is likely that the same set of problems occur in the group of doubtful cases (i.e. pulsars which show A/R effects at some frequencies but not in others). This strengthens our general conclusions that A/R effects are apparent in pulsar profiles.

In cases where A/R effects are seen between the core and conal components in pulsars, it implies that the core emission necessarily has to originate closer to the stellar surface than the conal emission (see e.g. G&Ga; Dyks et al. 2004). The delay emission heights obtained by equation (6) are essentially the conal emission heights with respect to the core emission. Alternatively, geometrical methods can be used to find the conal emission height r_{KG} as specified by equation (4). A comparison between the conal emission heights measured by these two methods is shown in Fig. 6. In this figure, the clear A/R cases are marked with filled circles, doubtful cases are marked with open circles and the so-called counterexamples are marked with stars. Note that many of the negative r_{AR} values in Fig. 6 correspond to the counterexamples in our sample. This plot can be compared to fig. 29 of BCW, where a similar effect is noted, although the delay heights there were measured from polarization observations and they used log–log axes. It is noteworthy

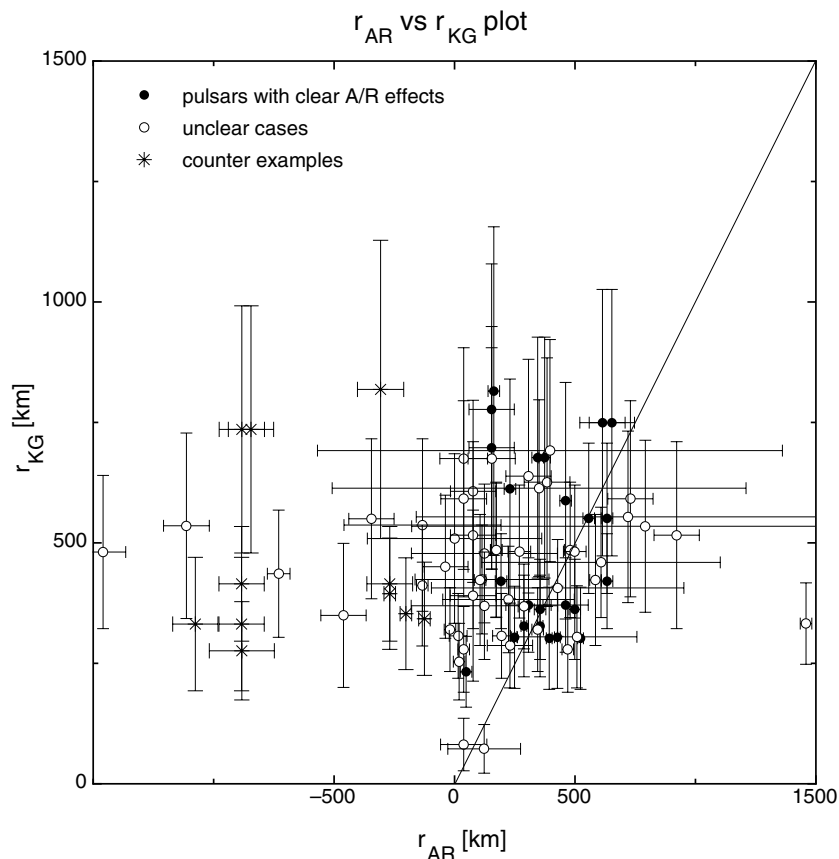


Figure 6. Relation between the delay emission height r_{AR} given by equation (6) and the semi-empirical geometrical height estimate r_{KG} given by equation (4). Note that statistically $r_{\text{KG}} > r_{\text{AR}}$ as seen by the excess of points lying above the $r_{\text{AR}} = r_{\text{KG}}$ line in the figure (see legend to distinguish different groups of pulsars). See text for details.

that statistically the relation $r_{\text{KG}} > r_{\text{AR}}$ seems to hold well. There are primarily two reasons that can explain this effect. First, the r_{AR} values can be underestimated if the putative core emission arises from a definite height above the polar cap. In order to square the two height estimates by making the cluster of points in Fig. 6 to be located on the 45° line, a nominal average core emission height of about 100 km is needed. Alternatively, the geometrical emission height r_{KG} might be overestimated, since the assumption prevailing in estimating these heights is that the measured widths entail the last open field lines, i.e. $s = 1$ (see equation 2). If the parameter s was around 0.7, the two height estimates would square with each other. As discussed by Mitra & Li (2004), a careful and systematic study of the relation of the core emission with respect to the PA traverse might help to resolve this issue.

ACKNOWLEDGMENTS

We thank the GMRT operational staff for observational support. The GMRT is run by the National Centre for Radio Astrophysics of the Tata Institute of Fundamental Research. We acknowledge the usage of the Gaussian-fitting program given to us by Michael Kramer, which has been extensively used in this paper. JG and JK acknowledge partial support of the Polish Grant N N203 2738 33. JK and KK acknowledge the Polish Grant N 203 021 32/2993. This paper was also partially supported by the Polish Grant N N203 3919 34. We would like to thank an anonymous referee whose comments and suggestions helped us improve our paper. We thank Urszula Maciejewska for critical reading of the manuscript.

REFERENCES

- Blaskiewicz M., Cordes J. M., Wasserman I., 1991, *ApJ*, 370, 643 (BCW)
 Dyks J., Rudak B., Harding A. K., 2004, *ApJ*, 607, 939
 Gangadhara R. T., 2005, *ApJ*, 628, 923
 Gangadhara R. T., Gupta Y., 2001, *ApJ*, 555, 31 (G&Ga)
 Gil J. A., Kijak J., 1993, *A&A*, 273, 563
 Gil J., Gronkowski P., Rudnicki W., 1984, *A&A*, 132, 312
 Gould D. M., Lyne A. G., 1998, *MNRAS*, 301, 235 (GL98)
 Gupta Y., Gangadhara R. T., 2003, *ApJ*, 584, 418 (G&Gb)
 Gupta Y., Gothoskar P., Joshi B. C., Vivekanand M., Swain R., Sirothia S., Bhat N. D. R., 2000, in Kramer M. Wex N., Wielebinski N., eds, ASP Conf. Ser. Vol. 202. Pulsar Astronomy – 2000 and Beyond. Proceedings of the 177th Colloquium of the IAU held in Bonn, Germany, 30 August – 3 September 1999. Astron. Soc. Pac., San Francisco, p. 277
 Gupta Y., Gil J., Kijak J., Sendyk M., 2004, *A&A*, 426, 229
 Kijak J., Gil J., 1997, *MNRAS*, 288, 631
 Kijak J., Gil J., 1998, *MNRAS*, 299, 855
 Kijak J., Gil J., 2003, *A&A*, 397, 969
 Kijak J., Kramer M., Wielebinski R., Jessner A., 1997, *A&A*, 318, L63
 Kramer M., Wielebinski R., Jessner A., Gil J. A., Seiradakis J. H., 1994, *A&AS*, 107, 515
 Lyne A. G., Manchester R. N., 1988, *MNRAS*, 234, 477
 Malov I. F., Suleimanova S. A., 1998, *Astron. Rep.*, 42, 388
 Mitra D., Deshpande A. A., 1999, *A&A*, 346, 906
 Mitra D., Li X. H., 2004, *A&A*, 421, 215
 Mitra D., Rankin J. M., 2002, *ApJ*, 577, 322
 Mitra D., Rankin J. M., 2008, *MNRAS*, 385, 606
 Mitra D., Rankin J. M., Gupta Y., 2007, *MNRAS*, 379, 932
 Mitra D., Rankin J. M., Sarala S., 2008, 40 Years of Pulsars: Millisecond Pulsars, Magnetars and More. AIP Conf. Proc., Vol. 983, Am. Inst. Phys., New York, p. 106
 Rankin J. M., 1983, *ApJ*, 274, 333
 Rankin J. M., 1986, *ApJ*, 301, 901
 Rankin J. M., 1990, *ApJ*, 352, 247
 Rankin J. M., 1993a, *ApJ*, 405, 285
 Rankin J. M., 1993b, *ApJS*, 85, 145
 Radhakrishnan V., Cooke D. J., 1969, *Astrophys. Lett.*, 3, 225
 Sirothia S., 2000, MSc thesis, University of Pune
 Srothlik Z., Rankin J. M., 2005, *MNRAS*, 362, 1121
 Swarup G., Ananthakrishnan S., Kapahi V. K., Rao A. P., Subrahmanya C. R., Kulkarni V. K., 1991, *Curr. Sci.*, 60, 95
 Weltevrede P., Stappers B. W., Edwards R. T., 2006, *A&A*, 445, 243
 Weltevrede P., Edwards R. T., Stappers B. W., 2007, *A&A*, 469, 607

SUPPORTING INFORMATION

Additional Supporting Information may be found in the online version of this article.

Appendix. Detailed description of all the pulsars that were analysed for the A/R effects.

Please note: Wiley-Blackwell are not responsible for the content or functionality of any supporting materials supplied by the authors. Any queries (other than missing material) should be directed to the corresponding author for the article.

This paper has been typeset from a $\text{\TeX}/\text{\LaTeX}$ file prepared by the author.